Exploring the local environment of the engineered nanoclay Mica-4 under hydrothermal conditions using Eu^{3+} as a luminescent probe

Rosa Martín-Rodríguez [a,b], Fernando Aguado [b,c], María D. Alba [d], Rafael Valiente [b,e], Esperanza Pavón [d,f], Ana C. Perdigón [a,b,*]

[a] Dpto. QUIPRE, Universidad de Cantabria, Avda. de Los Castros 46, 39005 Santander, Spain
[b] Grupo de Nanomedicina, IDIVAL, Avda. Cardenal Herrera Oria s/n, 39011 Santander, Spain
[c] Dpto. CITIMAC, Universidad de Cantabria, Avda. de Los Castros 48, 39005 Santander, Spain
[d] Instituto Ciencia de los Materiales de Sevilla, CSIC-US, Américo Vespucio 49, 41092 Sevilla, Spain
[e] Dpto. Física Aplicada, Universidad de Cantabria, Avda. de Los Castros 48, 39005 Santander, Spain
[f] Dpto. Física de la Materia Condensada, Universidad de Sevilla, Avda. Reina Mercedes, s/n, 41012 Seville, Spain

ARTICLE INFO

ABSTRACT

High charge mica $Na_4Al_4Si_4Mg_6O_{20}F_4$, Mica-4, is a promising candidate as a filling material to immobilize high-level radioactive waste in deep geological repositories due to its extraordinary adsorption capacity. In contrast to traditional clay materials, the structural composition of this mica, with a high content of aluminum in the tetrahedral sheet, enhances its chemical reactivity, favoring the formation of new crystalline phases under mild hydrothermal conditions, and thus providing a definitive isolation of the radionuclides in the engineered barrier. Moreover, this synthetic clay has some features that allow its use as an optical sensor by doping with luminescent rare earth cations such as Eu^{3+}. In this paper we discuss the local structure of the nanoclay Mica-4 using Eu^{3+} as a local probe to track the physical and chemical modifications under hydrothermal conditions. For that purpose, a set of hydrothermal experiments has been carried out heating Mica-4 and an aqueous $Eu(NO_3)_3$ solution in a stainless steel reactor at different temperatures and times. Optical properties of the as-treated samples were characterized by spectroscopic measurements. The fine peak structure of emission and the relative intensity of different Eu^{3+} transitions as well as the luminescence lifetime have been correlated with the structure and composition of this nanoclay, and the interaction mechanisms between the lanthanide ions and the clay mineral at different temperatures and times. Special attention has been paid to understanding the role of the aluminum content, which may act as either an aggregating or dispersing agent, in the optical features and reactivity of the system.

1. Introduction

The Environmental Protection Agency (EPA) defines nano-technology as the understanding and control of matter at dimensions of 1–100 nm [1]. Based on this definition, clay minerals are one of the most antiqueue nanomaterials used by the humanity for many different applications. In particular, clay minerals are the filling material chosen to seal tunnels in deep geological repositories (DGR), a multibarrier system designed to immobilize and store high-level radioactive waste [2]. The clay, as part of the engineered barrier, constitutes an ideal material for retarding the radioisotope diffusion to the environment due to its swelling ability, plasticity and adsorption capacity [3]. Several efforts have been made to develop new materials with a marked adsorption capacity, in order to enhance the retention role of the clay barrier. High charge micas, a synthetic family of swelling clays with a large cation exchange capacity (CEC), have been recently proposed as an alternative for radioactive waste immobilization [4]. Considering their layer charge, high charge micas belong to the true mica type (with two negative charges per unit cell) and to the brittle mica type aluminosilicates (with up to four negative charges per unit cell) [5]. In this context, the synthesis of the end-member of the Mica-4 family, with formula $Na_4Al_4Si_4Mg_6O_{20}F_4$ and 4 charges per unit cell, was a breakthrough in the field due to its particular structural and adsorption properties [6,7]. Specifically, synthetic Mica-4 presents: (1) a large theoretical CEC of 468 meq/100 g [8]; (2) unexpected structural stability despite its large negative charge density, opposite to brittle micas [9]; and (3) a Si/Al ratio close to one, breaking the generally accepted Lowenstein rule for aluminosilicates [4].

* Corresponding author.
E-mail address: perdigonac@unican.es (A.C. Perdigón).

Some studies have already confirmed the ability of this high charge mica to retain and immobilize radionuclides, constituting a definitive retention mechanism and super-selectivity for ^{137}Cs and [226]Ra in the interlayer space of Mica-4 [10,11].

Several mechanisms including surface adsorption, cation exchange reaction or colloidal precipitation are associated with the diffusion of the radionuclides through the clay engineered barrier. All of them highly dependent on the physical-chemical conditions of the surrounding underground water [12]. Furthermore, under subcritical conditions, new stable crystalline phases, mainly disilicates and aluminates, are generated by a chemical reaction between lanthanide or actinide cations and the silicate network, giving rise to a definitive permanent retention mechanism [13,14]. Several structural factors of the clay play an important role in its reactivity. In particular, a higher aluminum content and octahedral occupancy lead to a substantial improvement in reactivity [15]. In that sense, Mica-4 is a trioctahedral layered clay with all the octahedral sites occupied by magnesium and half of the silicon ions substituted by aluminum in the tetrahedral sheet, fulfilling the mentioned reactivity requirements. Previous studies on the interaction of lanthanide cations such as Eu^{3+} with Mica-4 under hydrothermal conditions have demonstrated the formation of new crystalline phases at temperatures as low as 150 °C [4]. Under subcritical conditions, the evolution of the Eu^{3+}/high charge mica system towards other crystalline phases is highly dependent on the hydrothermal conditions, namely time and temperature, and also the aluminum content.

Interestingly, Eu^{3+} cations have been intensively used as actinide simulators to evaluate the reaction processes between the clay material and radioactive actinides [16–19]. In addition, active radionuclides [153]Eu, [154]Eu and [155]Eu are minor elements in the spent nuclear fuel, although uranium is the principal component (*ca.* 95% of the spent nuclear fuel).

Trivalent lanthanides, and in particular Eu^{3+}, have also been used as luminescent local probes to analyze the crystalline structure and local site symmetry in diverse inorganic materials [20–23]. Das et al. [24] use Eu^{3+} to explore $Na_{0.1}Sr_{9.8}Eu_{0.1}(PO_4)_6F_2$ both as a potential phosphor material and host for radioactive waste immobilization. Moreover, the incorporation of the luminescent cation Eu^{3+} into the structure of the high charge mica with 2 charges per unit cell, Mica-2, has been previously used to monitor the long-term physical-chemical changes under mild hydrothermal conditions [25]. Eu^{3+} emission is a sensitive spectroscopic probe since the luminescence from both $^5D_0$ and $^5D_1$ excited states to all low-lying states as well as their emission lifetimes can be used to monitor the Eu^{3+} local environment [26]. Therefore, the diffusion of Eu^{3+} through the silicate network and the generation of new crystalline phases under hydrothermal conditions can be clearly differentiated. However, this spectroscopic method requires an optimal luminescence resolution, which is highly dependent on a set of structural characteristics of the host material. Firstly, in high charge micas, contrary to other natural clays, both the presence of few hydroxyl groups and the absence of impurities such as iron prevent emission quenching due to non-radiative multiphonon relaxation or energy transfer to luminescence killers. Secondly, the role of the aluminum, homogeneously distributed in the tetrahedral sheet of the aluminosilicate, plays an important role not only in the reactivity, but also in the optical properties of Eu^{3+}.

The layer charge of the aluminosilicate has been previously reported to be a limiting factor in the luminescence efficiency. Okada et al. [27] observed a decrease in the emission intensity with increasing exchange capacity, when a synthetic saponite and fluorotetrasilicic mica were compared. In that study, the decrease in luminescence intensity was attributed to Eu^{3+} aggregation. On the contrary, we have previously reported that in Mica-2 the aluminum, homogeneously distributed in the tetrahedral sheet and responsible

for the layer charge of the aluminosilicate, acts as an intrinsic dispersing agent that enhances Eu^{3+} luminescence [26]. Thus, there is an still open controversy regarding the effect of the high aluminum content and layer charge, on Eu^{3+} luminescence and lifetime. Consequently, although undesirable concentration quenching by aggregation of lanthanide ions in the clay network might occur, the application of Mica-4, a high charge mica with a potential adsorption capacity twice that of Mica-2 and with a layer charge value in the range of brittle micas, deserves careful evaluation.

In this work, we present an in-depth analysis of the reactivity and structural transformation of the Eu^{3+}/Mica-4 system, under hydrothermal conditions by spectroscopy. Different stages have been identified and correlated with previous x-ray diffraction (XRD) results during the adsorption process of Eu^{3+} cations under hydrothermal conditions. In particular, two main processes can be distinguished: (i) Surface adsorption in non-specific sites including diffusion of the cations in the bidimensional galleries of the Mica-4 by cation exchange reaction, and (ii) Modifications of the crystal field with specific sites generating new crystalline phases. Optical measurements, namely Eu^{3+} luminescence and lifetime, give complementary information of the local environment of the lanthanide cation before the generation of new crystalline phases, leading to a better understanding of the physical-chemical changes at short-range order. Special attention has been paid to understanding the role of the aluminum content and layer charge in both the reactivity and the spectroscopic features of the system.

2. Material and methods

2.1. Synthesis of high charge micas

A near-stoichiometric powder mixture with the following molar composition: (8-n) SiO_2, (n/2) Al_2O_3, 6 MgF_2, and 2 n NaCl was used to synthesize the Mica-n (n = 2 and 4) starting samples. The starting materials were SiO_2 from Sigma (CAS No. 112945–52–5 99.8% purity), $Al(OH)_3$ from Riedel-de Haën (CAS No. 21645–51–2, 99% purity), MgF_2 from Aldrich (CAS No. 20831–0, 98% purity), and NaCl from Panreac (CAS No. 131659, 99.5% purity). All reagents were mixed and ground in an agate mortar, and heated up to 900 °C in a Pt crucible in air for 15 h. After being cooled, the as-prepared solid was washed with deionized water and dried at room temperature.

2.2. Hydrothermal treatments

300 mg of the powdered Mica-n (n = 2 and 4) were dispersed in 50 ml of 5×10^{-2} M $Eu(NO_3)_3$ solutions in distilled water and heated up in a stainless steel reactor, at different temperatures (150, 200 and 300 °C) and times (0, 2, 14 and 30 days). The treatment at 0 days implies a heating ramp up to 300 °C, followed by cooling the sample down to room temperature. The reaction products were collected by filtering using a Millipore filter with 0.45 μm pore diameter, washed with distilled water, and dried in air at 60 °C overnight.

2.3. X-ray diffraction characterization

XRD patterns were obtained at the CITIUS X-ray laboratory (University of Seville, Spain) using a Bruker D8 Advance instrument equipped with a Cu Ka radiation source operating at 40 kV and 40 mA. Powder XRD patterns were obtained in the 2θ range of 3–70° with a step size of 0.015° and integration time of 0.1 s. Crystalline phase identification was carried out using the DIFFRACplus Evaluation package (©2010 Bruker AXS GmbH, Karlsruhe, Germany) and the ICDD PDF-4 + 2014 diffraction database.
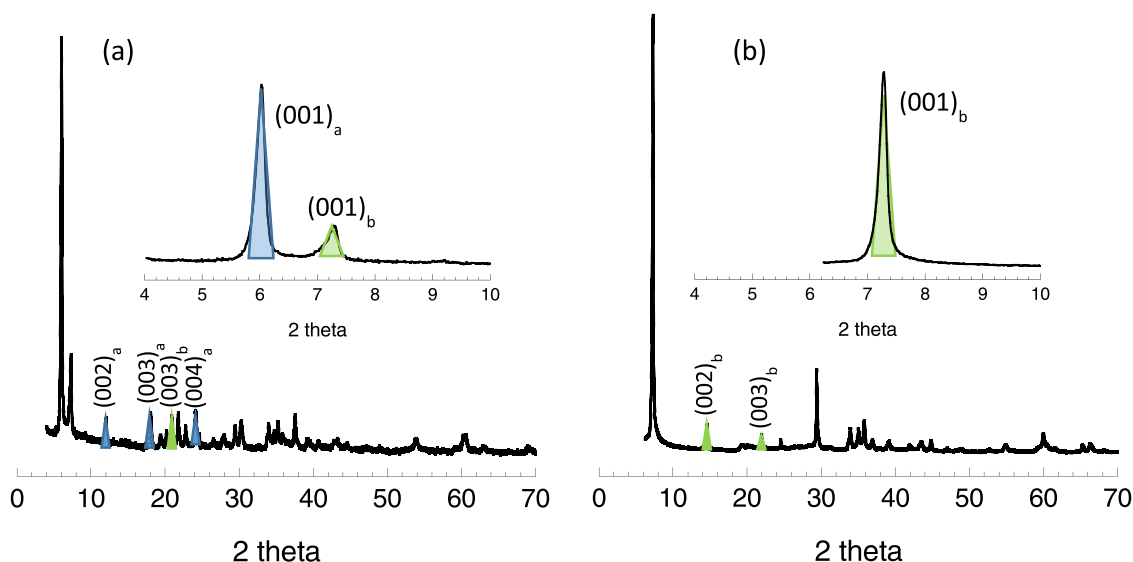
Fig. 1. XRD patterns of Mica-2 (a) and Mica-4 (b) hydrothermally treated with a Eu^{3+} aqua-solution at 300 °C 0 days.

2.4. Optical characterization

Emission, excitation and lifetime experiments were carried out using a FLSP920 spectrofluorometer (Edinburgh Inst.) equipped with double-monochromators, a 450 W continuous-wave Xe-lamp and a 60 W pulsed Xe-lamp for excitation, coupled with a Hamamatsu R928P photomultiplier tube for detection. All spectra were corrected for the system response.

3. Results and discussion

3.1. Structural and optical properties of Eu^{3+} in Mica-2 and Mica-4

Firstly, both Mica-2 and Mica-4 were hydrothermally treated at 300 °C for 0 days, for comparison purposes. Fig. 1 includes the XRD patterns of the as-treated Mica-2 and Mica-4 samples (PDF file card No: 00–054–1025). Since the basal spacing of high charge micas is highly dependent on both, the physical-chemical properties of the interlayer cation, such as the hydration energy and the electrostatic parameter, and also, on the value and origin of the layer charge of the aluminosilicate, the XRD technique has been extensively used to analyze the composition of the interlayer space [4,28].

The XRD pattern of Mica-2 exhibits two families of reflections, both characteristic of a mica-type layered structure. The first family includes an intense basal $(001)_a$ reflection at around $2\theta = 6°$ (d = 1.5 nm), attributed to a mica phase structure with Eu^{3+} cations located in the interlayer space of the phyllosilicate [26]. The second one, with a basal $(001)_b$ reflection at $2\theta = 7.2°$ (d = 1.2 nm), is associated to Na^+ cations accommodated in the hexagonal cavities of the tetrahedral sheet, and a pseudo-monolayer of water between the silicate layers [4]. Additionally, few low intensity peaks have been assigned to a magnesium silicate phase, forsterite (Mg_2SiO_4, PDF file card No: 00–34–0189). Taking into account previous reports, under these conditions of pressure and temperature, Eu^{3+} adsorption occurs in slightly higher amounts compared to the CEC of Mica-2, confirming that Eu^{3+}cations are adsorbed in the bidimensional galleries of the high charge mica [29].

On the contrary, the XRD pattern of Mica-4 under similar hydrothermal conditions, exhibits only one family of peaks corresponding to a mica-phase structure with the basal $(001)_b$ reflection at $2\theta = 7.2°$ (d = 1.2 nm), indicating that only hydrated monovalent cations are in the interlayer space of the aluminosilicate. Thus, the interlayer distance, a very sensitive parameter to ion exchange, is preserved during the Mica-4 treatment, and there is no evidence for the incorporation of Eu^{3+} cations in the interlayer of the aluminosilicate from XRD measurements. Forsterite reflections are also present in the XRD pattern. Recent studies revealed that the Eu^{3+} adsorption on the clay at 0 days is in the order of its CEC, as deduced by comparing the Eu^{3+} concentration in the initial solution and in the supernatant after the hydrothermal treatment, and it is ascribed to adsorption in non-specific sites of the silicate surface [29]. Furthermore, XRD confirms that the layered structure of the aluminosilicates is preserved during the treatment in both samples, as it can be deduced from the presence of different diffraction orders in the patterns.

Fig. 2 shows the luminescence spectra of the systems Eu^{3+}/Mica-2 (a) and Eu^{3+}/Mica-4 (b), after hydrothermal treatment for 0 days, and the temporal evolution of the Eu^{3+} $^5D_0 \rightarrow {}^7F_J$ Eu^{3+} luminescence intensity in Mica-2 (c) and Mica-4 (e). A schematic representation of Eu^{3+} exchanged or adsorbed in a high-charge mica-type aluminosilicate is also included (Fig. 2(d)).

In general, mica-type aluminosilicates are synthetic clays constituted by two tetrahedral SiO_4 sheets that sandwich an octahedral magnesium sheet. Isomorphous substitutions of Si^{4+} by Al^{3+} in the tetrahedral sheet originate a low negative charge density compensated by hydrated Na^+ in the interlayer space. Two interaction mechanisms between Eu^{3+} cations and the clay can be univocally distinguished during the hydrothermal treatments by analyzing the luminescence features of the sample, as demonstrated by our previous work in Mica-2 [25]. The first mechanism consists on both the adsorption of Eu^{3+} cations in non-specific sites on the surface of the clay and the cation exchange reaction in which the interlayer Na^+ is substituted by Eu^{3+}. The diffusion of the cations through the interlayer space mechanism is characterized by some particular photoluminescent properties, the presence of the green Eu^{3+} emission from the $^5D_1$ excited state being the most representative. In addition, the position and width of the formally forbidden $^5D_0 \rightarrow {}^7F_0$ transition are highly sensitive to the Eu^{3+} environment.

Interestingly, the transition energy of this band is centered at 578.7 nm (17,277 cm^{-1}) for hydrated Eu^{3+}, and the band is red-shifted for crystalline host matrices [21]. The shift to lower energies can be due to different effects, the main one is the change in the covalency of the metal-ligand bond and the mixing of states with different J values (J-mixing). The higher energy value for this transition would be expected for Eu^{3+} in the gas phase, 17374 cm^{-1}. The expansion of the electron cloud and the corresponding reduction of the interelectronic repulsion would lead to a red-shift of this
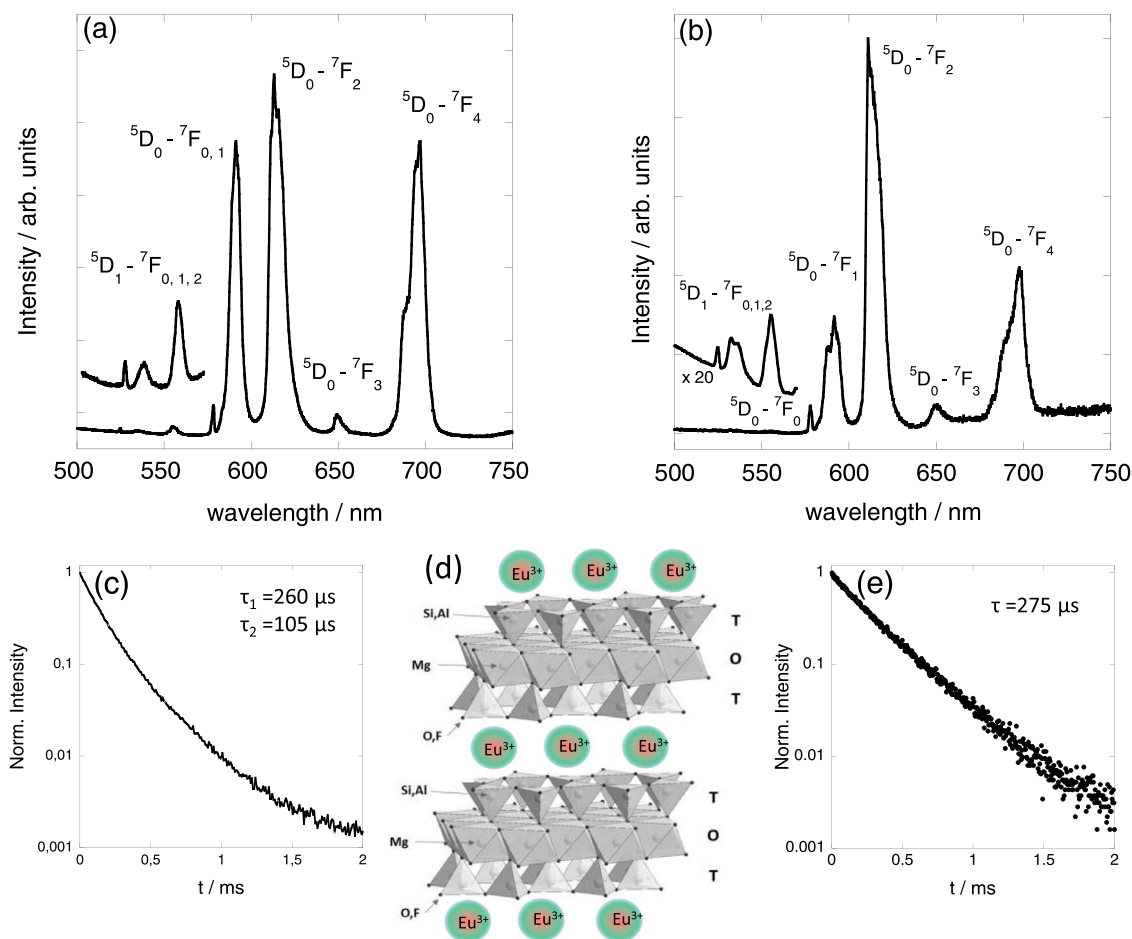
Fig. 2. Emission spectrum upon excitation at 393 nm of Eu^{3+} in the Mica-2 (a) and in the Mica-4 (b) heated with a Eu^{3+} aqua-solution at 300 °C for 0 days. Temporal evolution of the $^5D_0 \rightarrow ^7F_J$ Eu^{3+} emission intensity, recorded at 614 nm upon excitation at 393 nm for both samples (c) and (e), respectively. Representation of a Eu^{3+} exchanged high-charge mica-type aluminosilicate (d).

transition. However, off-diagonal matrix element contributes to the mixing of the $^5D_0$ and $^7F_0$ levels through the spin-orbit interaction increasing the energy difference. For instance, different values are reported for Eu^{3+} coordinated with water molecules, from 17255 to 17280 cm^{-1}. In fact, distinct empirical relationships have been derived between the $^5D_0 \rightarrow ^7F_0$ transition energy and the charge of ligands or the coordination number. Choppin and Wang correlated the shift of this transition with the number of ligands bound to Eu^{3+} [30]. Its energy decreases as the coordination number with water molecules increases. Finally, a single exponential decay for the $^5D_0$ Eu^{3+} excited state, with a value of ~250 µs, compatible with Eu^{3+} cations surrounded by water molecules in an inner-sphere conformation, is another characteristic of this adsorption mechanism [26]. The second process, a permanent retention immobilization, implies the generation of new crystalline phases in which the cation is covalently incorporated into the structure. The characteristic luminescent features of this second mechanism are the absence of the Eu^{3+} luminescence from the $^5D_1$ excited state, a shift of the $^5D_0 \rightarrow ^7F_0$ emission to higher wavelengths, and longer lifetime [25].

The luminescence spectrum of both samples (Fig. 2) consists of emission peaks assigned to transitions from both the $^5D_0$ and $^5D_1$ excited state to the ^7F_J (J=0–4) low-lying multiplets [21].

The observance in the emission spectra of a set of peaks located in the 500–570 nm range in the samples treated at 300 °C for 0 days that corresponds to the green Eu^{3+} emission from the $^5D_1$ energy level is consistent with the incorporation of Eu^{3+} cations in both high-charge micas. However, since the main interaction mechanism for the Mica-2 heated at 300 °C for 0 days is the incorporation of Eu^{3+}

into the interlayer space [25], the low intensity of the $^5D_1 \rightarrow 7 F_J$ Eu^{3+} emission bands, *ca.* 2 orders of magnitude weaker than the $^5D_0$ luminescence intensity in Mica-4, indicates that not significant amount of Eu^{3+} has entered into the interlayer space at these hydrothermal conditions. It is worth noting that Eu^{3+} cations do not diffuse in enough quantities to be detected by XRD techniques.

In this sense, luminescence measurements provide additional information related to the local environment of Eu^{3+} cations in the samples. As mentioned before, the energy associated to the $^5D_0 \rightarrow ^7F_0$ transition is extremely sensitive to the environment, being the corresponding transition energy 578.0 nm (17,300 cm^{-1}) for both Mica-2 and Mica-4 after 0 days treatment, close to the value of 578.8 nm (17,277 cm^{-1}) described for hydrated Eu^{3+}. Attending to the position of the $^5D_0 \rightarrow ^7F_0$ transition, the peak position for these samples is consistent with Eu^{3+} ions as aqua-complex.

The intensity ratio of the two transitions at about 617 nm ($^5D_0 \rightarrow ^7F_1$) and 593 nm ($^5D_0 \rightarrow ^7F_2$) is another feature that provides information about the Eu^{3+} local environment. Interestingly, the relative intensity of these transitions clearly infers differences in the evolution of Eu^{3+} adsorption after hydrothermal treatment in Mica-4 compared to the results previously described for Mica-2 [25]. I_{593}/I_{617} peak ratio is equal to 0.8 for Mica-2 and to 0.3 for both Mica-4 and the formed crystalline phases. The variation of the ratio is often used as a measure of the symmetry of the Eu^{3+} site, associated with changes in the second coordination sphere of europium [31]. This observation, points out the different adsorption mechanisms in Mica-2 and Mica-4, namely different contribution of surface adsorption, cation exchange reaction, as stated before. Finally, the

broadening of the $^5D_0 \rightarrow {}^7F_J$ transition bands in both spectra also reflects the low crystallinity of the samples probably due to some disruption of the silicate network during treatment and the different chemical surrounding of the Eu^{3+} ions.

The fine structure of the transition bands is perfectly resolved in both samples independently on the aluminum content and the layer charge value of the aluminosilicate. As introduced above and contrary to this observation, a high layer charge value has been previously associated with a loss of the luminescence, due to a quenching phenomenon caused by Eu^{3+} aggregation. This behavior has been described for a fluoro-tetrasilicic mica, a swelling mica with four negative charges per unit cell originated from octahedral lattice-site defects and without aluminum in its composition [27]. Thus, the improved luminescence properties exhibited by the high-charge micas analyzed in this work, Mica-2 and Mica-4, deserve a deep investigation of the structural parameters that modulate its optical properties, since they show great potential as photofunctional materials for different applications. Two fundamental compositional and structural characteristics of these samples may directly affect its luminescence and lifetime values. Firstly, the aluminum content. Tetrahedral Al^{3+} acts as an inherently dispersing agent of Eu^{3+} cations on the surface and in the interlayer space of high-charge micas, even when two tetrahedrally coordinated aluminum are adjacent, as it happens in Mica-4. Secondly, the origin of the layer charge. In high charge micas, the negative charge is localized in the tetrahedral sheet. On the contrary, when the layer charge is originated in the octahedral sheet, the deficit of charge is delocalized along the silicate structure, as it is the case for the fluoro-tetrasilicic mica. The decrease in the luminescence intensity in this fluoro-tetrasilicic mica has been attributed to Eu^{3+} aggregation [27].

Besides, the temporal evolution of the $^5D_0 \rightarrow {}^7F_J$ Eu^{3+} luminescence intensity is also displayed in Fig. 2(c) and (e). Two contributions with 260 µs and 105 µs lifetimes, are observed in Mica-2, while a single exponential contribution is identified in Mica-4, with 275 µs lifetime. A single exponential decay for the $^5D_0$ Eu^{3+} excited state, with a value of ~250 µs, compatible with Eu^{3+} cations surrounded by water molecules in an inner-sphere conformation, is another characteristic of a surface or interlayer adsorption mechanism as it has been aforementioned [26]. In addition, comparable lifetime values have been obtained for Eu^{3+} incorporated in Al_2O_3 and $Al(OH)_3$, 232 µs and 220 µs, respectively, suggesting that Eu^{3+} ions in high-charge micas are mainly in the form of inner-sphere conformation [31]. On the contrary, the lifetime values reported for Eu^{3+} ions adsorbed on other aluminosilicates, such as kaolinite (88 µs) and montmorillonite (85 µs), suggest an outer-sphere conformation [31]. Horrocks et al. [32] established a linear dependence between the inverse of Eu^{3+} lifetime and the number of coordinating water molecules. The longest lifetime observed in both samples can be ascribed to Eu^{3+} ions in a similar inner-sphere conformation, with 3 water molecules in the first coordination sphere. The second contribution in Mica-2, with a lifetime of 105 µs, can be attributed to free Eu^{3+} aqua-ion adsorbed on the mica in outer-sphere complexation. Since most Eu^{3+} cations are incorporated into the interlayer of Mica-2, Eu^{3+} cations stay attached on the surface of Mica-4, both in similar inner-sphere conformation. Under these experimental conditions, the high electrostatic layer attraction, due to the high aluminum content in the tetrahedral sheet of Mica-4, and the Eu^{3+} hydration enthalpy, limits the diffusion of chemical species through the interlayer space, thus preventing the cation exchange reaction mechanism. This retention mechanism constitutes a non-permanent immobilization in both samples, governed by attractive electrostatic forces.

3.2. Hydrothermal treatments of the Eu^{3+}/Mica-4 system

The effect of temperature and time on the adsorption capacity of Eu^{3+} by Mica-4 is investigated here in detail by studying the local
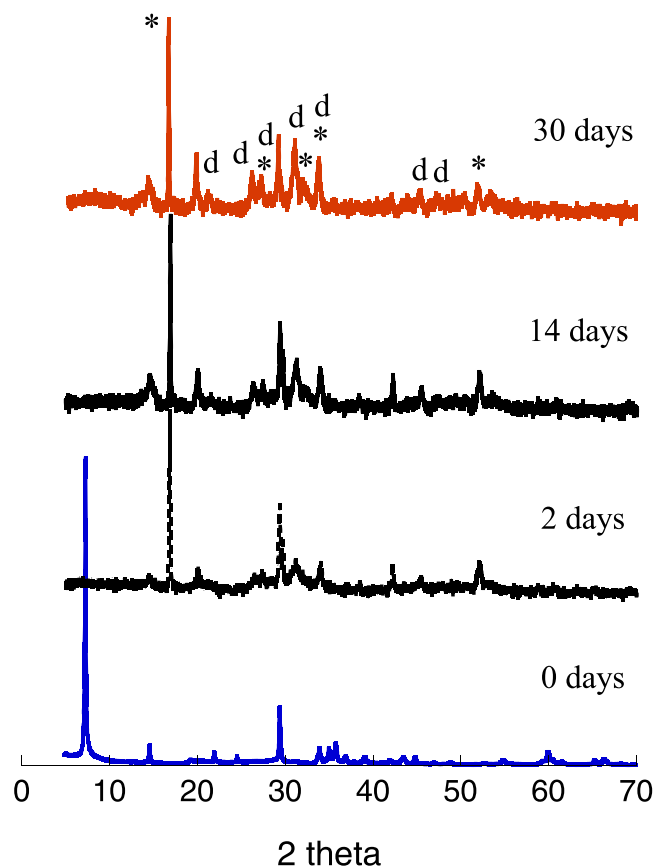

Fig. 3. XRD patterns of Mica-4 hydrothermally treated with an aqueous $Eu(NO_3)_3$ at different reaction times. $* = EuAlO_3$ (PDF 04–06–5193); d = F-$Eu_2Si_2O_7$ (PDF 00–23–984) or E-$Eu_2Si_2O_7$ (PDF 00–76–726).

environment of Eu^{3+} in the silicate network through luminescent measurements. In this study, an $Eu(NO_3)_3$ solution containing Mica-4 has been hydrothermally treated at different times and temperatures. Local changes are correlated to long-range order variations in the crystalline structure as determined by XRD [23]. Specifically, XRD patterns evidence a transformation from the clay structure to new crystalline phases under particular conditions, and this transformation is correlated with a modification of the optical features.

3.2.1. Influence of the reaction time

An aqueous $Eu(NO_3)_3$ solution containing Mica-4 was hydrothermally treated at a temperature of 300 °C in a time interval between 0 and 30 days. Fig. 3 includes the XRD patterns of Mica-4 after hydrothermal treatment at 300 °C at increasing reaction times. At 0 days, the XRD pattern is similar to the untreated Mica-4 sample, so not structural changes at long-range order can be inferred from the diagram. However, after 2 days of treatment, disruption of the layered structure of the clay, together with the appearance of small diffraction peaks due to the generation of new crystalline phases, mainly aluminates and disilicates, are evident. These new phases are growing with the reaction time.

Fig. 4 shows the excitation (a) and luminescence (b) spectra of the system Eu^{3+}/Mica-4 after hydrothermal treatment at 300 °C at different reaction times: 0, 2, 7, 14 days and up to 1 month. The excitation spectra were recorded detecting emission at 614 nm ($^1D_0 \rightarrow {}^7F_2$ Eu^{3+} transition) while luminescence spectra were obtained upon 393 nm excitation. Two different behaviors are distinguishable based on the optical features; the one detected for the initial sample, and the observed for treatments longer than 2 days.
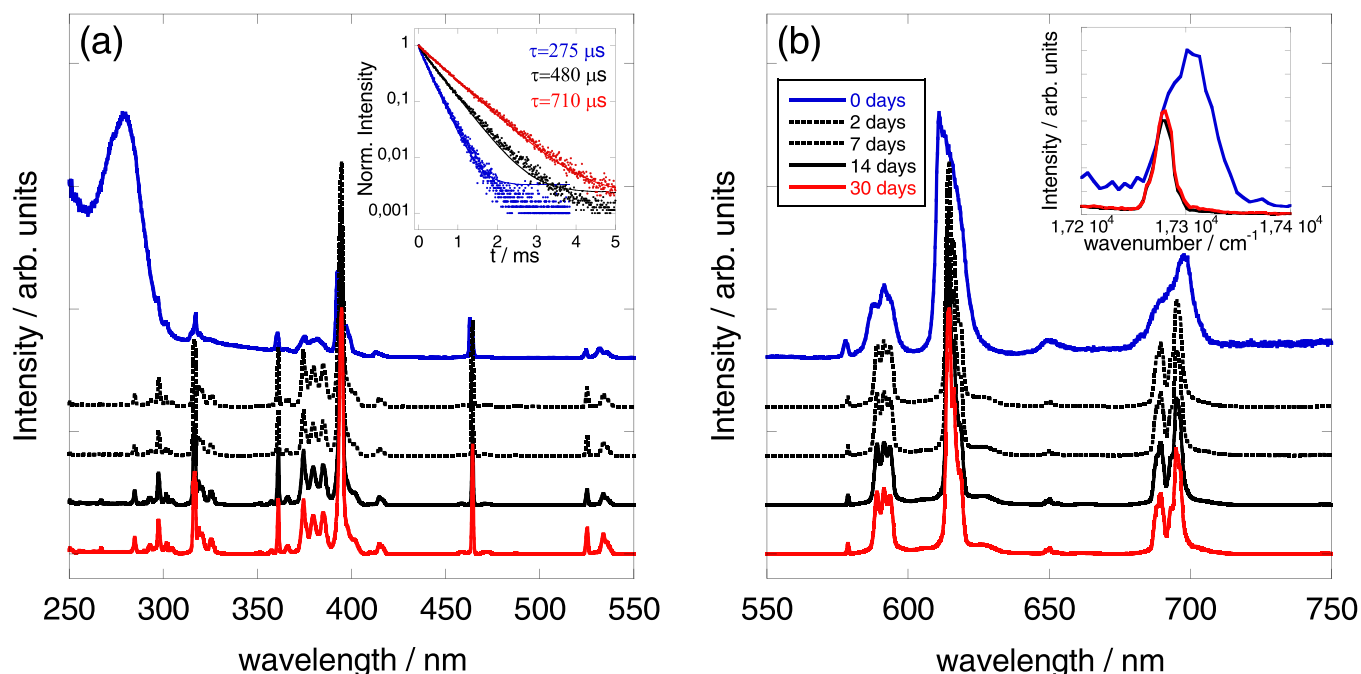
Fig. 4. (a) Excitation spectra of Mica-4 heated up with a Eu^{3+} aqua-solution at 300 °C at different times at 0, 2, 7, 14 and 30 days recording the emission at 614 nm and (b) emission spectra upon excitation at 393 nm. The inset in (a) displays the temporal evolution of the $^5D_0 \rightarrow {}^7F_J$ Eu^{3+} luminescence of Eu^{3+} for reaction times of 0, 14 and 30 days, after excitation at 393 nm and recorded at 614 nm. The inset in (b) shows the $^5D_0 \rightarrow {}^7F_0$ transition in wavenumber for 0 and 30 days.

Regarding excitation spectra, the broad excitation band located below 300 nm is only observed for the sample treated at 0 days, and it disappears for longer treatment times. When Eu^{3+} is linked to the H_2O or O^{2-} ligand, an electron transfer from the ligand to Eu^{3+} to form $Eu^{2+}-O^-$ is usually observed in the absorption and excitation spectra. This broad and intense charge transfer (CT) band is located around 240– 270 nm, depending on the host and environment of Eu^{3+}. Considering emission spectra, the observed peaks are assigned to Eu^{3+} transitions from the $^5D_0$ excited state to the ^7F_J ($J = 0$–4) low-lying multiplets. The weak emission from the $^5D_1$ Eu^{3+} excited state is absent after 2 days of treatment. The energy and the peak width associated with the $^5D_0 \rightarrow {}^7F_0$ emission, highly sensitive to the local environment of Eu^{3+}, is strongly dependent on the treatment time. Specifically, the band is shifted from 578.0 nm (17,300 cm^{-1}) for the sample treated at 0 days, to 578.7 nm (17,280 cm^{-1}) for longer treatments, associated to the formation of other crystalline phases (see inset in Fig. 3b). This redshift is accompanied by a decrease in the peak width, from 60 to 20 cm^{-1}. Attending the $^5D_0 \rightarrow {}^7F_{1,2,4}$ emission bands, the sample treated at 0 days exhibits broader peaks, while the samples treated at longer reaction times present well-resolved peaks. The splitting of the $^7F_1$ level for treatments longer than 2 days has been related to the Eu^{3+} ions in an orthorhombic or lower symmetry environment [33].

The temporal evolution of the $^5D_0 \rightarrow {}^7FF_J$ Eu^{3+} luminescence intensity recorded upon excitation at 393 nm of the system Eu^{3+}/Mica-4 after hydrothermal treatment at 300 °C for three selected reaction times is represented in the inset of Fig. 3(a). In contrast to the abrupt changes detected for both excitation and emission spectra, the lifetime increase with reaction time illustrates a continuous phase evolution during the hydrothermal treatments. The temporal dependence of the intensity for the sample at 0 days perfectly fits to a single exponential decay of 275 µs, evidencing a similar homogeneous distribution of Eu^{3+} ions within the Mica-4 structure, as previously described for other high-charge mica-type phases.

The decay curves for the samples treated at reaction times of 14 and 30 days provide lifetime values of 480 and 710 µs, respectively, the latter lifetime being ascribed to the formation of aluminate and disilicate crystalline phases, specifically $EuAlO_3$, $F-Eu_2Si_2O_7$ and $E-Eu_2Si_2O_7$ [29]. Previous studies have used lifetime measurements to identify the sorption behavior of Eu^{3+} onto different oxides including alumina (γ-Al_2O_3), gibbsite (α-$Al(OH)_3$), quartz (SiO_2) and solid amorphous silica, through a complexation mechanism either on aluminol or silanol sites [31]. In the case of Eu^{3+} sorption on alumina and gibbsite, the time dependence of the Eu^{3+} emission intensity fitted to a single lifetime of 220 µs at 25 °C. For quartz and amorphous silica two lifetimes were identified, a first specie with a lifetime of 130 µs and a second specie with a lifetime of 350 µs [31].

In summary, optical measurements confirm that the hydrothermal treatment at 300 °C of the system Eu^{3+}/Mica-4 induces the formation of new crystalline phases for a reaction time longer than 2 days.

According to luminescence and lifetime measurements, these crystalline phases grow up with time and remain practically constant at 1 month. The high aluminum content in the sample Mica-4 does not affect the quality of the luminescent measurements, because the negative charge in this synthetic mica is homogeneously distributed through the silicate layer. The aluminum in the structure of the aluminosilicate acts as a dispersing agent, preventing aggregation of the lanthanide ions. The reactivity of these high-charge micas is also highly dependent on the aluminum content. The charge deficit originated by substitution of silicon by aluminum in the tetrahedral sheet represents an active site for the nucleation of the new generated phases, starting from an electrostatic interaction between Eu^{3+} cations and Al^{3+} on the surface of the aluminosilicate. This represents a different mechanism compared to the one described for Mica-2, which was initiated by the incorporation of the Eu^{3+} cations in the interlayer space [25].

3.2.2. Influence of the reaction temperature

The effect of the second parameter, *i.e.* the temperature, on the optical properties of the system Eu^{3+}/Mica-4 after hydrothermal treatment has also been analyzed. The solutions have been hydrothermally treated at 150 °C, 200 °C and 300 °C for 1 month. Fig. 5 includes the temperature dependent XRD patterns.
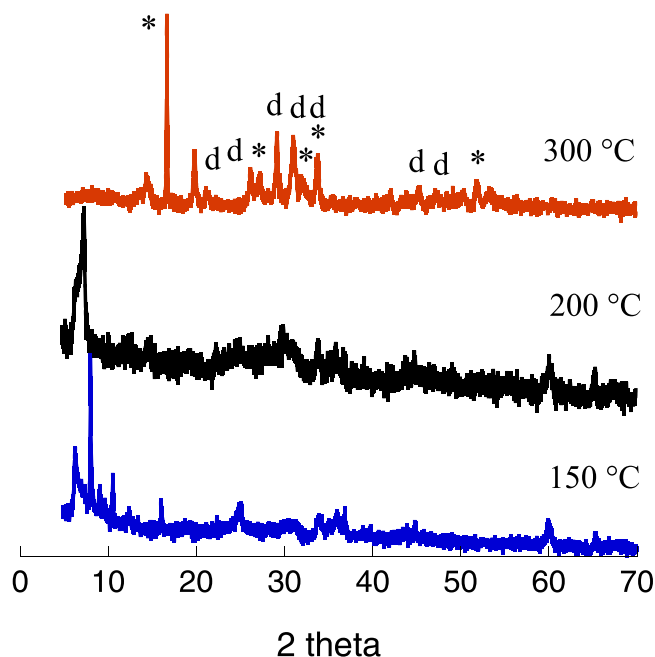
Fig. 5. XRD patterns of Mica-4 hydrothermally treated with an aqueous $Eu(NO_3)_3$ solution at different temperatures. * = $EuAlO_3$ (PDF 04–06–5193); d = F-$Eu_2Si_2O_7$ (PDF 00–23–984) or E-$Eu_2Si_2O_7$ (PDF 00–76–726).

Samples hydrothermal heated at 150 °C and 200 °C, present significant loss of the long-range order of the phyllosilicate structure after a month. Nevertheless, the layered structure is still maintained at those temperatures with broad *001* reflections, denoting that different hydration states of the interlayer cation coexist.

Fig. 6 includes the excitation spectra of Eu^{3+} recording emission at 611 nm, and the emission spectra upon excitation at 393 nm. The excitation spectra consist of peaks corresponding to Eu^{3+} *f-f*

transitions as assigned in Fig. 2a. The broad band centered at 280 nm is only observed for the samples treated at 150 ºC and 200 ºC. In the three luminescence spectra, the peaks corresponding to the $^5D_0 \rightarrow {}^7F_J$ Eu^{3+} transitions are also observed. However, differences in the peak width can be clearly observed. Firstly, the samples treated at 150 and 200 °C exhibit broader emission peaks, which is compatible with distorted Eu^{3+} cations adsorbed on Mica-4.

On the contrary, the sample treated at 300 °C presents sharper emission peaks, and this behavior has been previously related to the incorporation of the Eu^{3+} in the clay network through the formation of new crystalline phases, $EuAlO_3$ and $Eu_2Si_2O_7$ [29]. In this respect, the spectral shape of the $^5D_0 \rightarrow {}^7F_1$ emission in the sample heated at 300 °C displays three well-resolved peaks. The fact that three sublevels are observed for $^7F_1$ suggests that Eu^{3+} ions are in an orthorhombic or lower well-defined site-symmetry.

In addition, the spectra of the samples treated at 150 and 200 °C show weak Eu^{3+} green emission from the $^5D_1$ excited state. This emission has been associated to the diffusion of Eu^{3+} cations in the bidimensional galleries of the aluminosilicate or even on the surface. On the contrary, the sample treated at 300 °C for 1 month does not present these emission peaks, and the absence of this emission has been attributed to either multiphonon relaxation or cross-relaxation between Eu^{3+} neighbors, indicating stronger Eu^{3+}-Eu^{3+} interactions. Consistently, cross-relaxation is more likely to occur in the formed concentrated crystalline phases. Regarding the $^5D_0 \rightarrow {}^7F_0$ transition (see inset in Fig. 4b), the peak in the spectra of the samples treated at 150 and 200 °C is centered at 577.7 nm (17,310 cm^{-1}). This value is compatible with Eu^{3+} cations in an inner-sphere conformation, partially coordinated with basal oxygen of the aluminosilicate and water molecules, given the values reported for Eu^{3+} complexes in solution. Clearly, a different behavior is observed in the sample submitted at 300 °C, where the band corresponding to the $^5D_0 \rightarrow {}^7F_0$ transition appears shifted to 578.7 nm (17,280 cm^{-1}), an indication of the formation of new crystalline phases. Moreover, the peak width decreases from 51 cm^{-1} to 20 cm^{-1} with the temperature for samples treated from (150−200) °C to 300 °C indicating a better crystallinity or homogeneous environment.
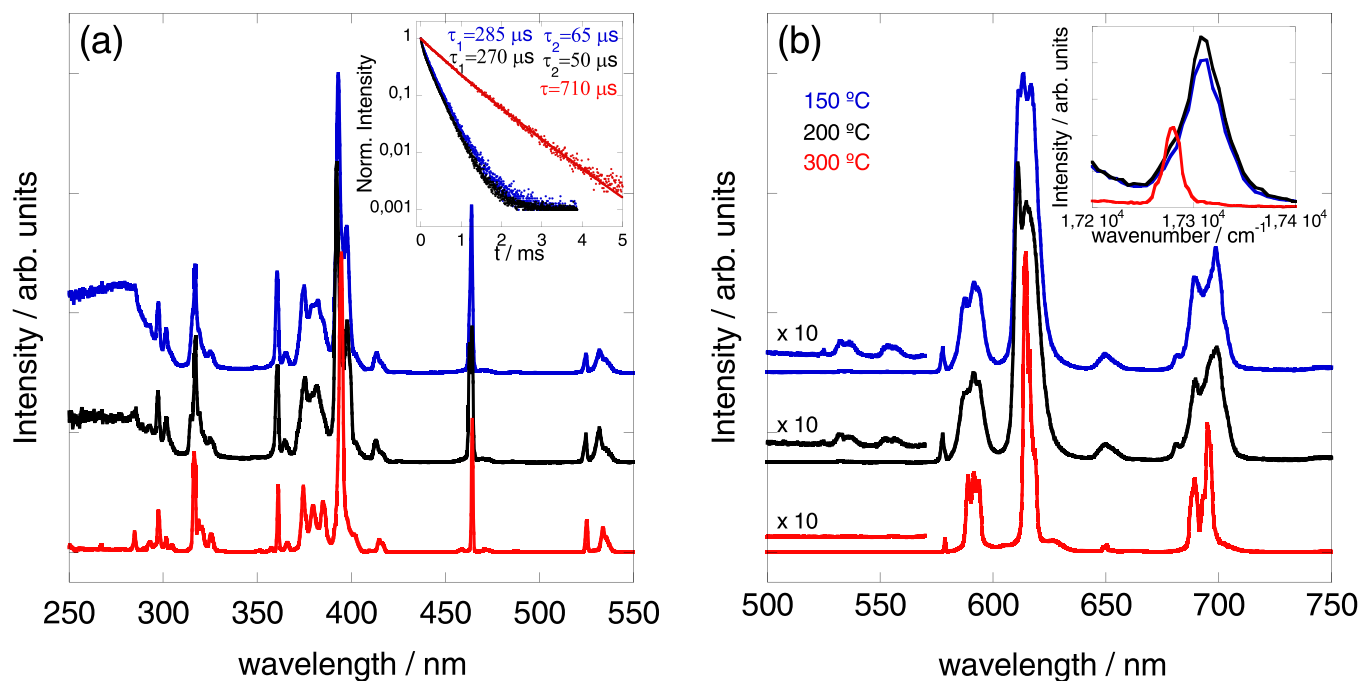
Fig. 6. Excitation spectra (detecting emission at 614 nm) (a) and emission spectra (exciting at 393 nm) (b) of the system Eu^{3+}/Mica-4 aqueous solution, treated at 150, 200 and 300 °C during 1 month. The inset in (a) shows the temporal evolution of the $^5D_0 \rightarrow {}^7F_J$ Eu^{3+} luminescence of Eu^{3+}-exchanged Mica-4 treated at 150, 200 and 300 °C for a month, after excitation at 393 nm and recorded at 614 nm. The inset in (b) depicts a detail of the $^5D_0 \rightarrow {}^7F_0$ emission in wavenumber.

Table 1

Optical features related to the physical-chemical interaction of Eu^{3+} cations with Mica-4.

Interaction mechanism	Optical features			
	$^5D_1 \rightarrow {}^7F_0$ green emission	$^5D_0 \rightarrow {}^7F_0$ peak position	$^5D_0 \rightarrow {}^7F_0$ peak width	$^5D_0 \rightarrow {}^7F_J$ lifetime value
Adsorption of Eu^{3+} in non-specific sites	Present[a]	$> 17,300 \text{ cm}^{-1}$	60 cm^{-1}	$\sim 275 \text{ μs}$
Generation of new crystalline phases	Absent	$17,280 \text{ cm}^{-1}$	20 cm^{-1}	$> 480 \text{ μs}$

[a] Related to a cation exchange mechanism.

The inset in Fig. 6a shows the temporal evolution of the $^5D_0 \rightarrow {}^7F_J$ Eu^{3+} emission intensity recorded upon excitation at 393 nm, for the Mica-4 after hydrothermal treatment with an Eu^{3+} aqueous-solution, during 1 month and different reaction temperatures, 150, 200 and 300 °C. The experimental curves for the samples treated at 150 and 200 ºC show a double-exponential behavior with lifetime values of $\tau_1 = 285$ μs and $\tau_2 = 65$ μs or $\tau_1 = 270$ μs and $\tau_2 = 50$ μs, respectively. The shortest lifetime values, τ_2, are comparable to the lifetimes observed for free Eu^{3+} aquo-complex. Thus, it indicates that several Eu^{3+} cations are adsorbed onto the silicate in an outer-sphere conformation. Besides, the longer lifetime values, τ_1, can be related to partially hydrated Eu^{3+} ions in an inner-sphere conformation. On the contrary, as mentioned above, the sample treated at 300 ºC shows a longer single-exponential decay ($\tau = 710$ μs) associated to the formation of aluminate and disilicate crystalline phases.

Finally, regarding the application of this Eu^{3+}-doped nanoclay for the immobilization and monitoring of radionuclides in the DGR, Table 1 summarizes the principal optical features, namely Eu^{3+} emission from $^5D_1$ excited state, position and width of the $^5D_0 \rightarrow {}^7F_0$ transition and $^5D_0$ emission lifetimes, useful to discriminate the physical-chemical interaction mechanism between the ions and Mica-4. A temporal or permanent immobilization of the radionuclides in the engineered barrier can be directly extrapolated from the mentioned parameters. The formation of new crystalline phases preserves the capture integrity in time and under temperature conditions. Specifically, an energy value associated to the $^5D_0 \rightarrow {}^7F_0$ transition of $17,300 \text{ cm}^{-1}$ or above, line width of the $^5D_0 \rightarrow {}^7F_0$ peak around 60 cm^{-1}, and $^5D_0$ Eu^{3+} emission lifetime values of ~ 275 μs evidence the adsorption of Eu^{3+} in non-specific sites on the clay surface.

All these features suggest a temporal retention mechanism of the radionuclides in the nanoclay. Additionally, the presence of the green Eu^{3+} emission from the $^5D_1$ excited state in the emission spectra is also correlated with a cation exchange mechanism or surface adsorption.

On the contrary, a redshift of the $^5D_0 \rightarrow {}^7F_0$ emission peak up to $17,280 \text{ cm}^{-1}$, together with a decrease of its line width up to 20 cm^{-1}, suggests a chemical reaction of the Eu^{3+} with the silicate network and the generation of new crystalline phases $EuAlO_3$, $F-Eu_2Si_2O_7$ and $E-Eu_2Si_2O_7$. These changes in the optical spectra are accompanied by longer lifetime values of the $^5D_0 \rightarrow {}^7F_J$ Eu^{3+} emission, ranging from 480 μs to 710 μs. This second mechanism represents a permanent immobilization of the radionuclides in the engineered barrier of the DGR.

4. Conclusions

In this work, we present in this work an in-depth study of the physical-chemical evolution of the nanoclay Mica-4 structure under mild hydrothermal conditions, using Eu^{3+} cations as atomic probe. High-charge micas fulfil the structural requirements to be used as an optical sensor, due to a low content of hydroxyl groups, insufficient to deactivate the Eu^{3+} emission, and the absence of impurities such as iron, responsible for luminescence quenching due to non-radiative relaxation. Furthermore, although the high CEC of the nanoclay could compromise the luminescence features of the Eu^{3+} emission by undesirable concentration quenching, the quality and resolution of the luminescent features is not affected by the high aluminum content in Mica 4. Two structural parameters have been identified as key modulators of the relevant optical properties for application as photofunctional material. (1) Isomorphic substitution of Si^{4+} by Al^{3+} in the tetrahedral sheet of the nanoclay, since aluminum acts as dispersing agent of the Eu^{3+} cations. (2) The origin of the negative charge in the tetrahedral sheet of the phyllosilicate. In addition, the influence of two fundamental parameters, time and temperature, on the evolution of the clay structure under hydrothermal treatment has been evaluated using optical measurements. Luminescent measurements can be used as a complementary technique to identify changes in the adsorption mechanism. After the treatment at 300 °C for 0 days, the Eu^{3+} cations are mostly adsorbed on the silicate surface, while the samples treated at times longer than 2 days incorporate the Eu^{3+} in the clay network through the formation of new crystalline phases. Similarly, treatments at 150ºC and 200ºC cause a temporal retention mechanism on the nanoclay surface, while transformation to new crystalline phases occurs in the sample treated at 300 ºC. Finally, this system, Eu^{3+}/Mica-4, shows great potential for application as engineered barrier with improved adsorption properties and as an *in situ* optical sensor for tracking the physical and chemical interactions of radionuclides with the clay in DGR.

CRediT authorship contribution statement

Rosa Martín-Rodríguez: Conceptualization, Investigation, Writing – original draft, Writing – review & editing. **Fernando Aguado:** Conceptualization, Investigation, Writing – original draft, Writing – review & editing. **María D. Alba:** Conceptualization, Investigation, Writing – original draft, Writing – review & editing. **Rafael Valiente:** Conceptualization, Investigation, Writing – original draft, Writing – review & editing. **Esperanza Pavón:** Conceptualization, Investigation, Writing – original draft, Writing – review & editing. **Ana C. Perdigón:** Conceptualization, Investigation, Writing – original draft, Writing – review & editing.

Data availability

Data will be made available on request.

Declaration of Competing Interest

The authors declare that they have no known competing financial interests or personal relationships that could have appeared to influence the work reported in this paper.

Acknowledgments

References

[1] S.S. Mukhopadhyay, Nanomaterial: look at the earth why clay ? Nat. Precedings (2011).

[2] B. Faybishenko, J. Birkholzer, D. Sassani, P.N. Swift, International Approaches for Deep Geological Disposal of Nuclear Waste: Geological Challenges in Radioactive Wast Isolation, (2016) 474.

[3] H.C.H. Darley, G.R. Gray, Composition and Properties of Drilling and Completion Fluids, Gulf Publishing Company, Houston, London, Paris, Zurich, Tokyo, 1988.

[4] M.D. Alba, M.A. Castro, M. Naranjo, E. Pavón, Hydrothermal reactivity of Na-n-micas (n = 2, 3, 4), Chem. Mater. 18 (2006) 2867–2872, https://doi.org/10.1021/cm0514802

[5] R.E. Grim, Clay Mineralogy, McGraw-Hill Book Company, New York, 1968.

[6] M. Park, D.H. Lee, C.L. Choi, S.S. Kim, K.S. Kim, J. Choi, Pure Na-4-mica: synthesis and characterization, Chem. Mater. 14 (2002) 2582–2589, https://doi.org/10.1021/cm0116267

[7] S. Komarneni, R. Pidugu, J.E. Amonette, Synthesis of Na-4-mica from metakaolinite and MgO: characterization and Sr2+ uptake kinetics, J. Mater. Chem. 8 (1998) 205–208, https://doi.org/10.1039/a706050e

[8] T. Kodama, S. Komarneni, Alkali metal and alkaline earth metal ion exchange with Na-4-mica prepared by a new synthetic route from kaolinite, J. Mater. Chem. 9 (1999) 2475–2480, https://doi.org/10.1039/a900113a

[9] A.C. Perdigón, D. Li, C. Pesquera, F. González, B. Ortiz, F. Aguado, C. Blanco, Synthesis of porous clay heterostructures from high charge mica-type aluminosilicates, J. Mater. Chem. A. 1 (2013) 1213–1219, https://doi.org/10.1039/c2ta00543c

[10] W. Paulus, S. Komarneni, R. Roy, Synthesis and selective exchange of strontium ions in Na4Mg6Al4Si4O20F4 mica, Nature 357 (1992) 571–573.

[11] S. Komarneni, N. Kozai, W. Paulus, Superselective clay for radium uptake, Nature 410 (2001) 771.

[12] H. Geckeis, J. Lützenkirchen, R. Polly, T. Rabung, M. Schmidt, Mineral-water interface reactions of actinides, Chem. Rev. 113 (2013) 1016–1062, https://doi.org/10.1021/cr300370h

[13] M.D. Alba, M.A. Castro, P. Chaín, S. Hurtado, M.M. Orta, M.C. Pazos, M. Villa, Interaction of Eu-isotopes with saponite as a component of the engineered barrier, Appl. Clay Sci. 52 (2011) 253–257, https://doi.org/10.1016/j.clay.2011.02.027

[14] M.D. Alba, P. Chain, M.M. Orta, Rare-earth disilicate formation under deep geological repository approach conditions, Appl. Clay Sci. 46 (2009) 63–68, https://doi.org/10.1016/j.clay.2009.07.012

[15] M.D. Alba, A.I. Becerro, M.A. Castro, A.C. Perdigón, Hydrothermal reactivity of Lu-saturated smectites: Part II. A short-range order study, Am. Mineral. 86 (2001) 124–131, https://doi.org/10.2138/am-2001-0113

[16] A. Bauer, T. Rabung, F. Claret, T. Schäfer, G. Buckau, T. Fanghänel, Influence of temperature on sorption of europium onto smectite: The role of organic contaminants, Appl. Clay Sci. 30 (2005) 1–10, https://doi.org/10.1016/j.clay.2005.02.001

[17] M.A. Ruiz-Fresneda, M. Lopez-Fernandez, M.F. Martinez-Moreno, A. Cherkouk, Y. Ju-Nam, J.J. Ojeda, H. Moll, M.L. Merroun, Molecular binding of EuIII/CmIIIby S tenotrophomonas bentonitica and its impact on the safety of future geodisposal of radioactive waste, Environ. Sci. Technol. 54 (2020) 15180–15190, https://doi.org/10.1021/acs.est.0c02418

[18] H. Wu, B. Ma, J. Chen, Z. Su, Y. Ji, S. Lin, D. Xu, M. Kang, Insight into the adsorption of europium(III) on muscovite and phlogopite: Effects of pH, electrolytes, humic substances and mica structures, Chemosphere 282 (2021) 131087, https://doi.org/10.1016/j.chemosphere.2021.131087

[19] Z. Sun, Y. gui Chen, Y. jun Cui, W. min Ye, Adsorption of Eu(III) onto Gaomiaozi bentonite corroded by cement waters: Effect of cement solutions on the long-term sorption performance of bentonite in the repository conditions, J. Clean. Prod. 251 (2020) 119692, https://doi.org/10.1016/j.jclepro.2019.119692

[20] M.D. Baker, M.M. Olken, G.A. Ozin, Laser-Induced fluorescence, far-infrared spectroscopy, and luminescence quenching of europium zeolite Y: site-selective probes of extraframework cations, J. Am. Chem. Soc. 110 (1988) 5709–5714, https://doi.org/10.1021/ja00225a022

[21] K. Binnemans, Interpretation of europium(III) spectra, Coord. Chem. Rev. 295 (2015) 1–45, https://doi.org/10.1016/j.ccr.2015.02.015

[22] C.Y. Morassuti, S. Finoto, J.R. Silva, L.A.O. Nunes, Y. Guyot, G. Boulon, M.L. Baesso, A.C. Bento, J.H. Rohling, S.M. Lima, L.H.C. Andrade, Combination of broad emission bands of Ti3+,4+/ Eu2+,3+ co-doped OH− free low silica calcium aluminosilicate glasses as emitting phosphors for white lighting devices, J. Alloy. Compd. 853 (2021) 155898, https://doi.org/10.1016/j.jallcom.2020.155898

[23] C.Y. Morassuti, L.H.C. Andrade, J.R. Silva, A.C. Bento, M.L. Baesso, F.B. Guimarães, J.H. Rohling, L.A.O. Nunes, G. Boulon, Y. Guyot, S.M. Lima, Eu2+,3+/Pr3+ co-doped calcium aluminosilicate glass for tunable white lighting devices, J. Alloy. Compd. 817 (2020), https://doi.org/10.1016/j.jallcom.2019.153319

[24] P. Das, N. Pathak, B. Sanyal, S. Dash, R.M. Kadam, Exploring Na0.1Sr9.8Eu0.1(PO4) 6F2 both as a potential phosphor material and host for radioactive waste immobilization, J. Alloy. Compd. 810 (2019) 151906, https://doi.org/10.1016/j.jallcom.2019.151906

[25] R. Martín-Rodríguez, F. Aguado, M.D. Alba, R. Valiente, A.C. Perdigón, Eu 3+ Luminescence in High Charge Mica: An in Situ Probe for the Encapsulation of Radioactive Waste in Geological Repositories, ACS Appl. Mater. Interfaces 11 (2019) 7559–7565, https://doi.org/10.1021/acsami.8b20030

[26] R. Martín-Rodríguez, F. Aguado, R. Valiente, A.C. Perdigón, Highly efficient photoluminescence from isolated Eu3+ ions embedded in high-charge mica, J. Mater. Chem. C. 5 (2017) 10360–10368, https://doi.org/10.1039/c7tc01818e

[27] T. Okada, Y. Ehara, M. Ogawa, Adsorption of Eu3+ to smectites and fluoro-tetrasilicic mica, Clays Clay Min. 55 (2007) 348–353, https://doi.org/10.1346/CCMN.2007.0550402

[28] E. Pavón, M.A. Castro, A. Cota, F.J. Osuna, M.C. Pazos, M.D. Alba, Interaction of hydrated cations with mica-n (n = 2, 3 and 4) surface, J. Phys. Chem. C. 118 (2014) 2115–2121, https://doi.org/10.1021/jp4110695

[29] M. José García-Jiménez, A. Cota, F.J. Osuna, E. Pavón, M.D. Alba, Influence of temperature and time on the Eu3+ reaction with synthetic Na-Mica-n (n=2 and 4), Chem. Eng. J. 284 (2016) 1174–1183, https://doi.org/10.1016/j.cej.2015.09.077

[30] G.R. Choppin, Z.M. Wang, Correlation between ligand coordination number and the shift of the 7F0-5D0 transition frequency in europium(III) complexes, Inorg. Chem. 36 (1997) 249–252, https://doi.org/10.1021/ic9500220

[31] E. Tertre, G. Berger, E. Simoni, S. Castet, E. Giffaut, M. Loubet, H. Catalette, Europium retention onto clay minerals from 25 to 150 °C: experimental measurements, spectroscopic features and sorption modelling, Geochim. Cosmochim. Acta 70 (2006) 4563–4578, https://doi.org/10.1016/j.gca.2006.06.1568

[32] W.H. William De, D.R. Sudnick, Lanthanide ion probes of structure in biology. laser-induced luminescence decay constants provide a direct measure of the number of metal-coordinated water molecules, J. Am. Chem. Soc. 101 (1979) 334–340, https://doi.org/10.1021/ja00496a010

[33] C.R. García, L.A. Diaz-Torres, J. Oliva, G.A. Hirata, Green EuAlO3:Eu2+ nanophosphor for applications in WLEDs, Opt. Mater. (Amst.). 37 (2014) 520–524, https://doi.org/10.1016/j.optmat.2014.07.016